# Proliferation of SH-SY5Y neuroblastoma cells on confined spaces

**Ewelina Kalwarczyk[1,✉], Agnieszka Lukasiak[1], Damian Woznica[1], Weronika Switlik[2], Julia Anchimowicz[2], Piotr Zielonka[1], and Slawomir Jakiela[1,✉]**

[1]Department of Physics and Biophysics, Institute of Biology, Warsaw University of Life Sciences, 159 Nowoursynowska Street, 02776 Warsaw, Poland
[2]Department of Biochemistry and Microbiology, Institute of Biology, Warsaw University of Life Sciences, 159 Nowoursynowska Street, 02776 Warsaw, Poland

**Ensuring proper cell growth in systems with limited space, such as in microfluidic technologies, is essential for consistent culture comparisons and results. In this report, we mainly present the proliferation of SH-SY5Y cells on circular polycarbonate chambers with different surface areas. We selected SH-SY5Y cells due to their widespread application in the study of neurodegenerative diseases. Our research showed a clear link between the dish's surface area and the rate of cell growth. It is significant that cell growth in chambers with a diameter of 10 mm or more matches that of a standard dish culture. Observations showed that as the chamber diameter decreased, SH-SY5Y cells had noticeably slower growth, even with the same initial seeding density. Furthermore, we compared the effects on HeLaGFP cells, which exhibited similar behaviour to SH-SY5Y cells, and 16HBE14$\sigma$ cells, which showed efficient proliferation at various diameters. Additionally, we checked the development of SH-SY5Y cells in a sealed chamber of 12 mm diameter to observe their growth under limited gas exchange conditions. Cell proliferation was continuously monitored using a real-time microscope to capture dynamics. The results indicated that the observed cell growth was comparable to that of standard culture dishes.**

**SH-SY5Y | Cell proliferation | Polycarbonate chambers | Morphological changes | Oxygen consumption rate**

**Correspondence:** ***ewelina_kalwarczyk@sggw.edu.pl, slawomir_jakiela@sggw.edu.pl***

DRAFT

## Introduction

Traditional microscopic studies in cell biology and bioengineering use fixed biological preparations, which are the gold standard for assessing the impact of compounds on cell function and viability (1). However, this approach inherently limits the ability to observe dynamic processes occurring in real time. With the aid of microfluidic technology, we can easily combine microscopic inspection with precise drug delivery(2, 3). This breakthrough makes it possible to continuously monitor the influence of different toxins or drugs on cell function(4). To go even further, organ-on-a-chip systems work like real tissue systems and show how they react to disease (5, 6).

The authors wanted to use microfluidic techniques to study SH-SY5Y cells, which were picked as a model for neurodegenerative diseases(7, 8). In basic research into neurodegenerative diseases, the choice of an appropriate model system is crucial(9, 10). Both human and animal cells are used, including primary and immortalised cell lines. The human immature neuroblastoma cell line SH-SY5Y, widely used in Parkinson's and Alzheimer's disease research(11, 12), can be modified to mimic dopaminergic(13, 14) or cholinergic(15, 16) states. These features make it valuable for studying toxic protein aggregation(17, 18) and mitochondrial dysfunction(19, 20). In our early tests, however, growing SH-SY5Y cells in small microfluidic chambers (made of polycarbonate, PDMS, and glass substrates with and without surface modification) slowed their growth rate more than 10 times compared to standard dishes. Therefore, we conducted a series of calibration studies to identify the ideal chamber size for achieving cell proliferation similar to what we observed in conventional culture dishes.

The studies here give us very interesting information about how SH-SY5Y cells grow in carefully made polycarbonate chambers with diameters ranging from 3 mm to 50 mm. Importantly, we used these chambers without any additional surface treatment to enhance cell adhesion. A comparative analysis of cell growth in these chambers versus conventional 60-mm-diameter Petri dishes (Corning) was performed. All images capturing the coverage of the test media during successive days of culture are available in the Zenodo repository(21). Real-time monitoring of cell growth was achieved using a phase-contrast microscope, and growth kinetics were methodically analysed by extensive examination of microscopic images.

We also studied SH-SY5Y cell respiration using the Oroboros Oxygraph-2k device. The aim of this study was to explain how a population of cells in a sealed chamber without gas exchange consumes oxygen in the culture medium. We investigated the growth of SH-SY5Y cells over a one-week observation period in a hermetic polycarbonate chamber, specifically designed for targeted studies in microfluidic systems. In addition, a video showing the growth of SH-SY5Y cell cultures, with individual culture frames recorded every 5 minutes, has been deposited in the Zenodo repository(22).

Research in the fields of cell biology and bioengineering appears to be important, especially as we move the culture into small microfluidic systems. These systems offer remarkable opportunities for observing cellular responses to drugs in the diseases being studied(4). However, they also present a significant challenge for cell function in confined spaces(23), a point highlighted in this article.

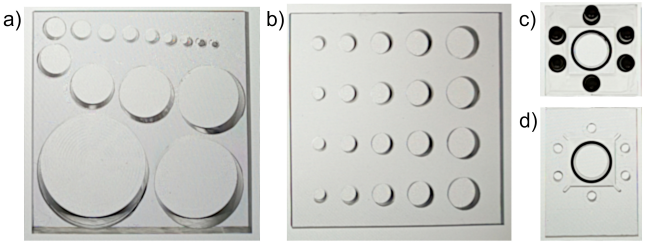


**Fig. 1.** Photographs depicting a custom-designed multi-chamber culture dish carefully crafted from polycarbonate using CNC milling are presented herein. The culture dish comprises the following components: a) A 15-well multi-chamber with varying chamber diameters ranging from 2.4 to 50 mm. The diameters include: 2.4, 3, 4, 5, 6, 7, 8, 9, 10, 15, 20, 25, 30, 40, and 50 mm. b) A 20-well chamber featuring diameters of 6, 8, 10, 12, and 15 mm. Notably, each diameter is replicated four times, facilitating comparative experiments. c) The top layer and d) the bottom layer of a hermetically sealed polycarbonate chamber with a diameter of 12 mm are also showcased. These chambers were sealed using an O-ring and secured together with 6 M3 screws.

## Materials and methods

**Materials.** The following chemicals and solutions were provided by Sigma-Aldrich, Germany: Dulbecco's modified Eagle's medium (DMEM) - D6546, Eagle's minimum essential medium (MEM) - M4655, heat inactivated fetal bovine serum (FBS) - F9665, L-glutamine solution, 200 mM - G7513, antibiotics solution containing 10 000 units of penicillin, 10 mg/mL streptomycin - P0781, MEM Non-Essential Amino Acid (NEAA) - M7145, Trypsin-EDTA solution - T3924, sodium dodecyl sulphate (SDS) - L3771, dichloromethene – 650463, Oligomycin - O4876, carbonyl cyanide 4-(trifluoromethoxy)phenylhydrazone (FCCP) - C2920, rotenone - R8875, and antimycin A - A8674. Ethyl alcohol, 96% was obtained from POCH, Poland (396420113), phosphate buffered saline (PBS) without calcium and magnesium was purchased from Lonza.

**Cells.** Three cell lines were used in a controlled laboratory environment to study cellular responses. The initial cell line, SH-SY5Y human neuroblastoma, was obtained from ECACC and cultured in DMEM with 10% FBS, 1% 200 mM L-glutamine, 1% antibiotic solution and 1% NEAA for optimal growth and viability.
In addition, the study included the Milipore 16HBE14$\sigma$ human bronchial epithelial cell line, which was cultured in MEM with 10% FBS and 1% antibiotics solution to diversify cellular components and increase the breadth of the study.
A third cell line, HeLaGFP inducible GFP HeLa stable, purchased from GenTarget Inc., was cultured in DMEM with 10% FBS, 1% 200 mM L-glutamine and 1% antibiotics solution.
Cell growth was continuously monitored using an Olympus CKX53 phase-contrast microscope with a DLT camera (Delta Optical, DLT-Cam PRO 1080 HDMI USB) in a temperature-controlled chamber set at 37 °C as per experimental requirements.

**Chambers.** In our investigation, cellular cultures were cultivated in diverse vessels, encompassing commercially available cell culture dishes, such as NUNC Easy Flasks (75 $cm^2$) obtained from Thermo Scientific. Additionally, we employed 60 mm petri dishes from Corning. Taking a more tailored approach, our research incorporated the use of specially designed multi-chamber cultures (see Figure 1). These chambers were carefully crafted with precision by milling 10 mm and 5 mm thick polycarbonate plates (Makrolon, Bayer, Leverkusen, Germany) using a state-of-the-art CNC milling machine (MSG4025, Ergwind, Gdansk, Poland). To mitigate evaporation of the medium and emulate conditions akin to a standard Petri dish for cell culture, these chambers were fitted with a polycarbonate lid.

## Experimental

**Fabrication of multi-chamber cell dish.** In order to enhance the prepared culture dishes, their surfaces underwent a smoothing process facilitated by a methylene chloride vapor stream. Following this, they were carefully cleansed using a solution of 0.1 M SDS, ethyl alcohol, and deionized water. Ultimately, the dishes underwent a comprehensive sterilization procedure, which entailed roasting them in an oven at 110 °C for 10 hours and subjecting them to UV light for 30 minutes within a laminar flow clean bench.

**Growth of SH-SY5Y cells in polycarbonate culture dish.** In this investigation, a freshly prepared cell suspension, characterized by a known cell concentration per milliliter using Bio-Rad's TC20 automated cell counter, was uniformly distributed across all chambers of the culture dish. The volume of the cell suspension was carefully adjusted to maintain a consistent liquid height of approximately 2 mm in each chamber, ensuring a uniform cell surface density measured in cells per square centimeter.
The prepared culture dishes were then placed in a cell culture incubator set at 37 degrees C with a 5% $CO_2$ concentration. The growth of the culture was systematically observed in all the polycarbonate chambers, as well as in the other bottles and dishes mentioned, using a phase-contrast microscope. For each culture plate, five microscope images were taken - one at the centre of the plate and four at random locations. After image acquisition, the culture plate was returned to the incubator, allowing continuous and prolonged monitoring of cell growth. Microscopic image analysis allowed the average surface coverage of the culture plate to be determined over time. This analytical approach remained consistent throughout the majority of the experiments, unless explicitly stated otherwise.
Throughout the growth process, typically extending up to 7 days, the culture medium remained unchanged unless specific alterations were mandated for a particular experiment.

**Measurement of the oxygen consumption rate (OCR).** To elucidate the oxygen consumption rate (OCR) in SH-SY5Y cells, we used a Clark-type oxygen electrode, following the mitochondrial function assessment protocol described in a previously published methodology(24). SH-SY5Y cells were grown in NUNC Easy Flasks (75 $cm^2$), each containing 12 ml of culture medium, to approximately 90% con-

DRAFT

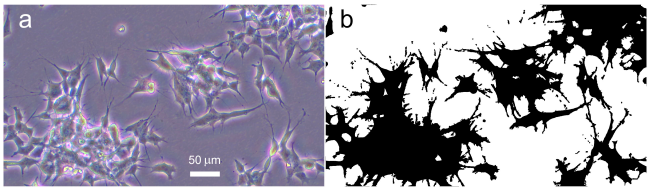


**Fig. 2.** Phase-contrast microscope image of SH-SY5Y cells (a) together with corresponding binarized picture (b).

fluence (equivalent to approximately 10 million cells per flask). A suspension of SH-SY5Y cells in culture medium at concentrations of 1 million/ml and 2.5 million/ml was then added to the measuring chambers of the Oxygraph-2K system (Oroboros Instruments, Austria).

For the determination of the non-phosphorylating leak, 4 mg/ml oligomycin, an inhibitor of mitochondrial ATP synthase, was used to reflect the maximal coupled state of the mitochondria. To achieve maximum uncoupling of the electron transfer system (ETS), 1 mM FCCP (carbonyl cyanide 4-(trifluoromethoxy)phenylhydrazone) was used. The residual oxygen consumption was then determined by adding 2.5 mM rotenone and 0.5 mM antimycin A, inhibitors of complex I and III of the ETS, respectively.

The expected oxygen consumption time was estimated from the initial oxygen concentration values and the baseline OCR of the cells.

**Metodology of data collection.** In order to characterise the developmental trajectory of cells within chambers of varying dimensions, cell images taken on different days of culture were binarised. This was done either manually using the GNU Image Manipulation Program (GIMP) software or semi-automatically using the Phantast phase-contrast microscopy segmentation toolbox in ImageJ. Phantast-binarised images were then manually refined using the GIMP where necessary.

Quantification of cell-covered areas was performed using ImageJ. The resulting values from each set of images were averaged, resulting in mean confluence measurements at different stages of the cell culture. An illustrative representation of SH-SY5Y cells under phase contrast microscopy is shown in Figure 2a, while the corresponding binarised representation is given in Figure 2b.

**Monitoring SH-SY5Y cell growth in a hermetically sealed polycarbonate microfluidic chip over a one-week period.** This investigation employs biological microscopy techniques to provide real-time insights into the dynamic transformations and growth trajectories of SH-SY5Y cells within a carefully controlled microenvironment. The resulting images, taken at five-minute intervals, were processed and condensed into a comprehensive video using ImageJ, as detailed in the Zenodo repository(22). The hermetically sealed chip design provides a precisely controlled environment, maintaining a constant temperature throughout the microscopic observation and eliminating the need to move the chip. This design choice allows for accurate monitoring and comprehensive documentation of cell behaviour, interactions and growth patterns over a predetermined one-week period.

The chip used, which is an integral part of the research, comprises two intricately interconnected polycarbonate components, securely screwed together and sealed with O-rings - as shown in Figure 1c, d. Prior to assembly, all elements underwent a thorough cleaning process and were annealed at 110 °C for 10 hours. After extensive sterilisation under UV light for 30 minutes in a laminar clean bench, the individual components were assembled. A 0.3 ml chamber (12 mm diameter) was then filled with a cell suspension containing 1 x $10^5$ cells/ml. Prior to microscopy, the culture was pre-incubated at 37 °C, 5% $CO_2$ for 24 hours. The chamber was securely positioned within the microscope chamber and a constant temperature of 37 °C was maintained without $CO_2$ control. At this point, real-time monitoring of SH-SY5Y cell growth began.

## Results and discussion

**Exploring seeding concentration effects on SH-SY5Y cell growth dynamics.** The investigation into the impact of seeding concentration on cell growth, particularly focusing on SH-SY5Y cells cultured in 60 mm Petri dishes at three different concentrations ($1 \times 10^4$, $5 \times 10^4$, and $1 \times 10^5$ cells/ml), provides valuable insights into the kinetics of cell proliferation. This study utilized four separate culture plates for each concentration to ensure robustness and reliability in the results. The data in Figure 3a shows a clear link between

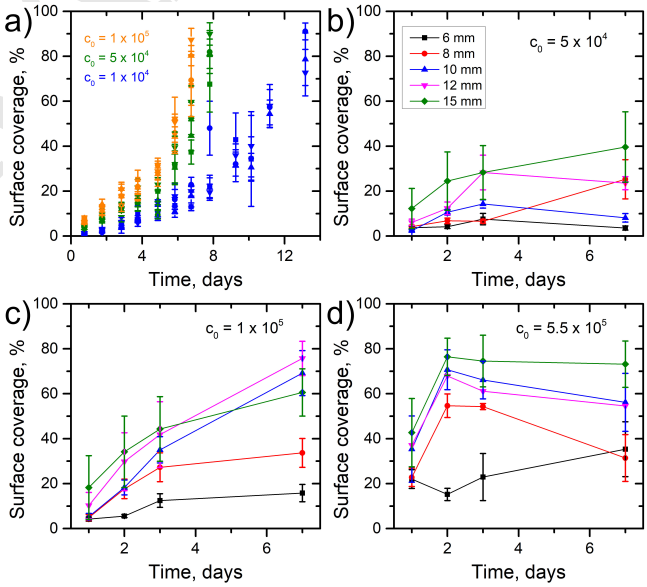


**Fig. 3.** (a) The growth curve shows the proliferation of SH-SY5Y cells in a 60 mm culture plate, initially seeded at three different concentrations. (b) - (d): Growth curves of SH-SY5Y cells at different cell diameters at different seeding concentrations. The colour-coded chamber diameters in panel (b) correspond to those in panels (c) and (d).

seeding concentration and cell proliferation rates. The microscopic images were carefully inspected to determine the culture plates' average surface coverage over time. SH-SY5Y cells' exponential growth dynamics are particularly noteworthy.

DRAFT

A key discovery from this study is the direct association between seeding concentration and the rate at which full confluence occurs. At the greatest seeding concentration of $1 \times 10^5$ cells/ml, the cells reach complete confluence in just 7 days. However, achieving full confluence at a lower seeding concentration of $1 \times 10^4$ cells/ml takes around 2 weeks.

This observation aligns harmoniously with the prevailing literature regarding cell culture and proliferation dynamics. According to an exhaustive study(25, 26), heightened seeding concentrations have consistently shown a direct correlation with an accelerated cell growth rate and a reduced time to confluence across diverse cell lines. The study underscores the critical importance of precisely adjusting seeding density to achieve better outcomes in cell culture.

Furthermore, the investigations conducted by Johnson et al.(27) and Nirmalanandhan et al.(28) posit that increased seeding concentrations hold the potential to amplify cell proliferation rates. This phenomenon is potentially attributed to heightened cell-cell interactions and increased resource availability. Their findings robustly reinforce the notion that elevated seeding concentrations can indeed enhance cell proliferation rates.

In conclusion, the study seems to offer meaningful insights into the impact of seeding concentration on the growth patterns of SH-SY5Y cells. The findings suggest a clear link between the initial number of cells and their proliferation rate, which appears to be in harmony with existing research on the topic. This knowledge is likely important for improving cell culture practices and for establishing more effective and consistent conditions for cell growth in future experiments.

**Investigating the impact of available surface area on the growth of SH-SY5Y cells.** In our pursuit to uncover the influence of available surface area on the growth dynamics of SH-SY5Y cells, we innovatively designed and crafted polycarbonate multi-chamber culture dishes. These dishes were tailored to feature varied surfaces conducive to cell proliferation, spanning from 0.07 $cm^2$ (in circular chambers with a 3 mm diameter) to 19.63 $cm^2$ (in circular chambers with a 50 mm diameter), see Figure 1a. The through preparation of these chambers, as detailed in the experimental section, ensured the experimental integrity.

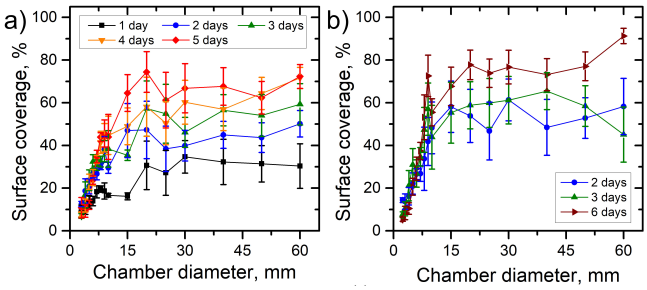


**Fig. 4.** Variations in surface coverage within cell chambers were observed in relation to chamber diameter for SH-SY5Y cells. The specific conditions, denoted by passage number and initial cell concentration, were as follows: a) SH-SY5Y p10, with an initial concentration of $1 \times 10^5$ cells/ml; b) SH-SY5Y p15, with an initial concentration of $5 \times 10^4$ cells/ml. Guidelines have been included to aid visual interpretation.

Accurate calculation of the cell suspension volume was carried out to achieve a uniform cell suspension height of 2 mm in each chamber, thereby establishing an equivalent average surface density of cells ($1 \times 10^4$ cells/$cm^2$ for a concentration of $5 \times 10^4$ cells/ml). After seeding, the dish was securely covered with a polycarbonate lid and incubated in a controlled cell incubator (37 degrees C / 5% $CO_2$). Using a phase-contrast microscope, we made periodic assessments of cell growth in the chambers every 1-2 days. The captured images showed dynamic changes in the mean cell confluence over time, according to the graphical analysis. Figure 4 illustrates an interesting relationship between the growth curve of SH-SY5Y cells and the area used for cell growth. In smaller chambers with a diameter below approximately 10 mm, surface coverage exhibits a proportional scaling with chamber size. Conversely, in chambers larger than 15 mm in diameter, surface coverage appears to be independent of chamber size, depending solely on the stage of culture growth. Notably, the average confluence remains consistently stable across all chambers with a diameter greater than 10 mm.

**Examining the impact of seeding concentration on SH-SY5Y cell growth.** In our study examining how the initial number of cells affects their growth in confined spaces, we closely monitored the growth of SH-SY5Y cells within chambers of different diameters (6, 8, 10, 12 and 15 mm), shown in Figure 1b, using different seeding concentrations ($5 \times 10^4$, $1 \times 10^5$ and $5.5 \times 10^5$ cells/ml). A consistent medium height of 2 mm was maintained throughout the study and microscopic images of the developing cell growth were taken at intervals of 1, 2, 3 and 7 days.

Analysis of the microscopy images, as shown in Figure 3b) - d), revealed several notable observations. Firstly, in chambers with a smaller diameter, such as 6 mm, cell aggregation appeared to be independent of seeding concentration. Despite an initial attachment of a substantial number of cells to the surface and their healthy appearance during the early stages of growth (observed at 1 and 2 days), only aggregated cells were visible after 3 days. Secondly, in intermediate size chambers (8 - 10 mm in diameter), a higher seeding concentration resulted in rapid cell growth followed by aggregation. Additionally, cell aggregation also occurred in intermediate-size chambers with low seeding concentrations. Finally, for chambers larger than 10 mm in diameter, a seeding concentration of $1 \times 10^5$ cells/ml proved optimal for maintaining long-term observation of cell growth.

**The growth of HeLaGFP and 16HBE14$\sigma$ cells in polycarbonate multichamber.** The growth of SH-SY5Y cells and their limited ability to adhere to surfaces, compared to other cell types, have been extensively studied by other researchers. Numerous factors, including substrate stiffness, integrin-mediated signaling, growth factors, and cell-cell interactions, have been identified as crucial in regulating the adhesive properties of SH-SY5Y cells (29, 30).

Motivated by these findings, we sought to compare the growth patterns of the more adherent 16HBE14$\sigma$ and HeLaGFP cells within polycarbonate chambers subjected to

DRAFT

experimentation (Figure 1a). The cell seeding process involved introducing cells from suspension at a concentration of $1 \times 10^5$ cells/ml. Our study involved daily, precise microscopic examinations to observe how cells were growing. The resulting growth curves, elucidated in Figure 5, offer a comprehensive depiction of the temporal evolution of cell proliferation within this experimental framework.

Our study showed that the growth of HeLaGFP cells, similar to SH-SY5Y cells, is influenced by chamber size, with a decreasing effect observed for chambers larger than 10 mm in diameter. In contrast, 16HBE14$\sigma$ cells did not show a clear growth dependence on chamber diameter. In particular, smaller chambers (diameter < 6 mm) resulted in reduced coverage after 4 days compared to 3 days for both cell lines. Nevertheless, both cell lines exhibited rapid growth, reaching 90% confluence after 4 days. Interestingly, 16HBE14$\sigma$ cells showed faster growth in polycarbonate chambers compared to HeLaGFP cells.

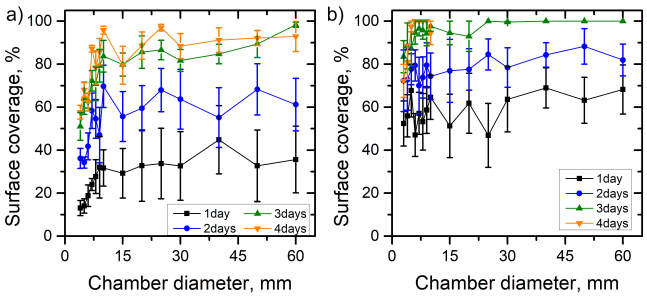


**Fig. 5.** Temporal evolution of cell growth: tracking the expansion of HeLaGFP (a) and 16HBE14$\sigma$ (b) cell populations over time, depicted as surface coverage relative to chamber diameter. The cells were initially seeded at concentration $1 \times 10^5$ cells/ml.

**The SH-SY5Y cells show low mitochondrial function expressed as OCR .** The mitochondrial functionality within SH-SY5Y cells is distinguished by a low oxygen consumption rate (OCR), as delineated in Figure 6. The reduced respiratory activity in SH-SY5Y cells is likely due to their unique neuronal characteristics, increased sensitivity to oxidative stress, and possible mitochondrial issues. This is shown by lower levels of ATP, mitochondrial membrane potential (MMP), and citrate synthase activity(31, 32).

In this investigation, we sought to elucidate the oxygen consumption dynamics exhibited by SH-SY5Y cells during the process of cellular respiration. The baseline OCR for a concentration of 1 million SH-SY5Y cells per milliliter was determined to be approximately 8.8 pmol/(s*ml). Following the introduction of oligomycin, an ATP synthase inhibitor, we limited the flow of protons back into the mitochondrial matrix. This intervention resulted in a marked reduction in cellular oxygen consumption, with OCR falling to 8.5 pmol/(s*ml). Following the administration of FCCP, a compound known for uncoupling the mitochondrial electron transport system (ETS), cellular respiration reached its zenith at 10.4 pmol/(s*ml). Statistical analysis revealed no significant variance between the effects induced by FCCP and the baseline OCR, or the OCR observed during ETS with inhibited ATP synthase (post-oligomycin administration). Notably, when employing a 2.5-fold higher cell concentration, the OCR subsequent to FCCP administration exceeded that following oligomycin administration by more than twofold. Crucially, the baseline OCR showed a 2.5-fold escalation with increasing cell concentration, confirming a linear correlation between OCR and cell concentration. In the final phase of the cellular respiration study, we evaluated the inhibition of complexes I and III in the ETS using rotenone and antimycin A, respectively. Employed in tandem, these compounds effectively impeded the flow of electrons throughout the entire electron transport chain, facilitating the measurement of extra-mitochondrial oxygen consumption.

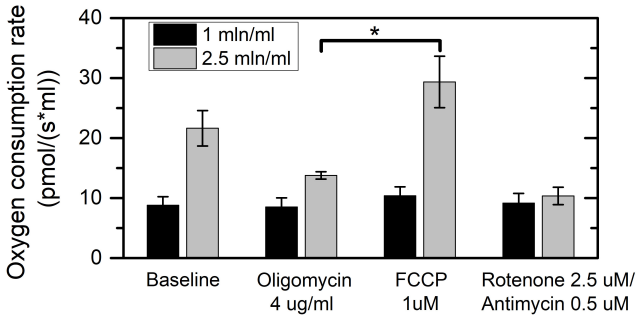


**Fig. 6.** Oxygen consumption rate in SH-SY5Y cells: The depicted bars illustrate the OCR for two cell concentrations — $1 \times 10^6$ cells/ml (black bars) and $2.5 \times 10^6$ cells/ml (grey bars). Results are presented as means ± standard error of the mean (SEM), with a sample size of $n = 4$ for the former and $n = 3$ for the latter. Statistical significance, denoted by (*), was determined at p < 0.05 using one-way analysis of variance (ANOVA).

**Table 1.** Anticipated duration of oxygen utilization by SH-SY5Y cells at varied abundances in the culture medium, assuming no air exchange. The presented table displays results averaged to two significant digits. Abbreviations: $O_2$ conc. - initial oxygen concentration in the culture medium; OCR - oxygen consumption rate; OCT - oxygen consumption time.

| | $10^4$ cells/ml | $10^6$ cells/ml |
|---|---|---|
| $O_2$ conc. (pmol/ml) | 220000 | 220000 |
| OCR (pmol/s*ml) | 0.088 | 8.8 |
| OCT (s) | 2500000 | 25000 |
| OCT (min.) | 42000 | 420 |
| OCT (h) | 700 | 7 |
| OCT (days) | 29 | 0.29 |

The expected duration of oxygen consumption for different concentrations of SH-SY5Y cells is shown in Table 1. Specifically, the approximate time for oxygen consumption is 29 days for a cell concentration of $10^4$ cells/ml and 2.9 days for a concentration of $10^6$ cells/ml. These results are consistent with the baseline Oxygen Consumption Rate (OCR) exhibited by the cells as shown in Figure 6. It is important to note that the estimated oxygen consumption time was derived from a linear relationship and did not control for cell division. To improve the accuracy of our understanding of oxygen consumption, it is important to include the rate of cell division when calculating the corrected OCR. In addition, the diffusion of oxygen within the polycarbonate system should be carefully considered to ensure a more accurate representation of the overall oxygen dynamics in the experimental setup.

DRAFT

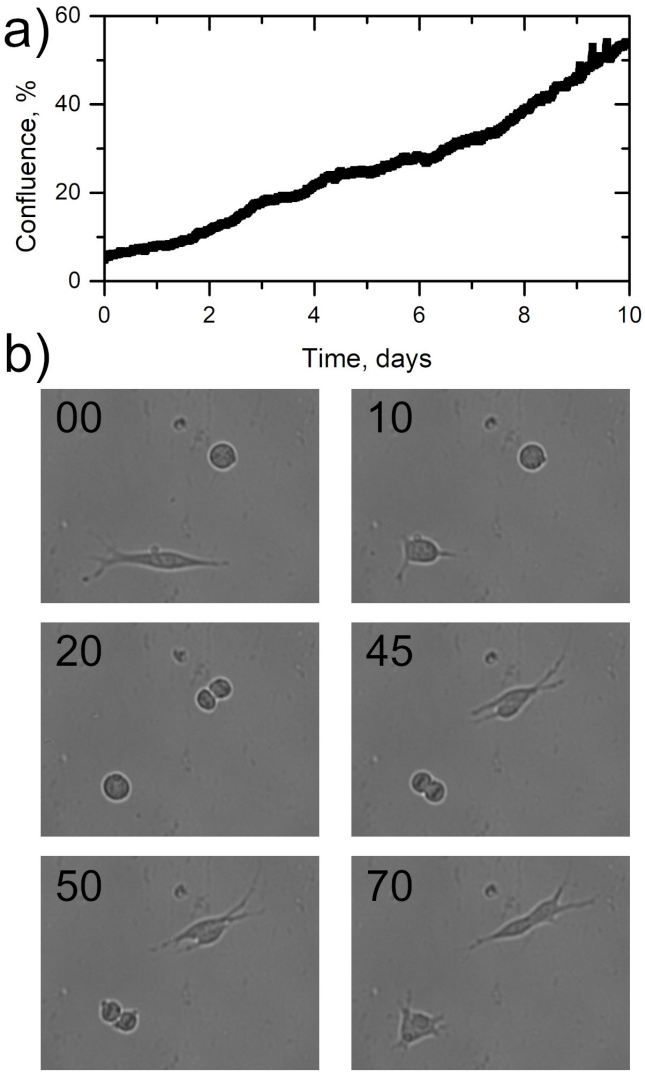


**Fig. 7.** a) The graph illustrates the temporal evolution of surface coverage within the on-chip chamber. b) The cultivation of SH-SY5Y cells is depicted, revealing discernible morphological transformations—from an elongated surface configuration to a spherical shape—and the distinctive positioning of chromosomal lines within the cell both pre and post-division. Each individual image is temporally annotated in minutes, relative to the initial photograph.These individual frames are extracted from a video available in the Zenodo repository.(22)

**Long, real time microscopic observation of the growth of SH-SY5Y cells in sealed chamber.** In the initial phase of cultivating SH-SY5Y cells on microfluidic chips, the authors conducted preliminary tests using small chambers with a 0.5 mm diameter. Unfortunately, no observable cell growth was evident in these chambers. Subsequent investigations demonstrated a notable preference of SH-SY5Y cells for chambers with diameters exceeding 10 mm. Building upon these insights, a carefully designed, sealed chamber with a 12 mm diameter and a volume of 0.3 ml was crafted - compare Figure 1c, d. Continuous microscopic monitoring of SH-SY5Y cell growth dynamics within this chamber was then undertaken.

This study aimed to precisely track the real-time microscopic development of cells without external gas exchange. The chamber volume of 0.3 ml was chosen based on cellular respiration results and the requirement for observations spanning at least one week. Consequently, the chip's chamber exhibits a cell surface density of 200 cells/mm$^2$ at the outset. Figure 7a shows how the surface coverage in the chip chamber changes over time. Comparing a sealed 12 mm diameter chamber with a standard culture chamber, the area covered by cells was similar on days 2, 3 and 7 of the culture period, as shown in Figure 3c. This suggests that long-term cell culture without air exchange through the medium is comparable to conventional cell culture.

In addition, the morphological behaviour of SH-SY5Y cells during long-term culture was investigated (see Figure 7b). We observed the morphological transformation of a dividing cell from a stretched surface configuration to a spherical shape. The process of cell division is illustrated in Figure 7b20-b45, showing the positioning of chromosomes and the inclusion of temporal markers to indicate the dynamics of the process. After division, the spherical cells return to their stretched form on the surface. To our knowledge, this morphological feature of SH-SY5Y cell division has not yet been reported.

## Conclusions

Here, we examined how SH-SY5Y neuroblastoma cells grow in custom-designed chambers. Our initial findings showed that these cells grew more slowly in small chambers. As a result, we began a precise calibration process to determine the ideal chamber size.

The study investigated how the initial seed concentration affects cell growth rate. It found a clear connection between higher concentrations and faster cell proliferation, which aligns with existing research.

We also looked into how available surface area affected the growth of SH-SY5Y cells and found that polycarbonate chambers with a diameter of about 10 mm had the same rate of cell proliferation as standard 60 mm Petri dishes. This finding has important implications for improving cell culture techniques, as it suggests that smaller chambers create unfavourable conditions for cell proliferation. Although SH-SY5Y was the primary focus, HeLaGFP also showed similar patterns. In contrast, 16HBE14$\sigma$ cells showed no dependence on proliferation changes based on chamber diameter.

The study revealed that SH-SY5Y cells have low mitochondrial function, as evidenced by their reduced oxygen consumption rate. This unique respiratory property makes them ideal for long-term studies in sealed chambers. Observations support the practicality of culturing these cells in large, sealed plastic chambers (minimum diameter: 10 mm). The preference for rigid polymers over softer polymers, such as PDMS with higher gas permeability, streamlines experimental setups and increases the practicality of the microfluidic platform(33).

Additionally, we observed a morphological change in the shape of SH-SY5Y cells during cell division, from stretched to spherical. After division, the cells reverted to their original shape.

These findings seem important for researchers in fields such as neuroscience, cell biology, and bioengineering. They pro-

DRAFT

vide clear guidelines for improved experimental design and execution. The demonstrated adaptability of SH-SY5Y cells to different culture conditions opens up possibilities for novel research methods, contributing to the advancement of cellular research.

### AUTHOR CONTRIBUTIONS

EK: conceptualization, formal analysis, data curation, investigation, methodology, writing – original draft, and writing – review & editing; AL: formal analysis, data curation, investigation, methodology; DW: formal analysis, data curation, investigation, methodology; WS: formal analysis, data curation; JA: formal analysis, data curation; PZ: conceptualization, writing – original draft, and writing – review & editing; SJ: conceptualization, funding acquisition, investigation, methodology, project administration, resources, supervision, writing – original draft, and writing – review & editing.

### COMPETING FINANCIAL INTERESTS

There are no conflicts to declare.

### DATA AVAILABILITY STATEMENT

Two Zenodo repositories(21, 22) contain the original files used to prepare the figures and formulate the conclusions.


### ACKNOWLEDGEMENTS

This research was supported by funding provided by the Program SONATA BIS 9 of the National Science Centre, Poland, Grant No. 2019/34/E/ST4/00281.


## Bibliography


1. Jungwoo Lee, Meghan J. Cuddihy, and Nicholas A. Kotov. Three-Dimensional Cell Culture Matrices: State of the Art. *Tissue Engineering Part B: Reviews*, 14(1):61–86, March 2008. ISSN 1937-3368. doi: 10.1089/teb.2007.0150. Publisher: Mary Ann Liebert, Inc., publishers.
2. Samar Damiati, Uday B Kompella, Safa A Damiati, and Rimantas Kodzius. Microfluidic devices for drug delivery systems and drug screening. *Genes*, 9(2):103, 2018.
3. Alireza Arandian, Zeinab Bagheri, Hamide Ehtesabi, Shima Najafi Nobar, Neda Aminoroaya, Ashkan Samimi, and Hamid Latifi. Optical imaging approaches to monitor static and dynamic cell-on-chip platforms: A tutorial review. *Small*, 15(28):1900737, 2019.
4. Nihan Yonet-Tanyeri, Maher Amer, Stephen C. Balmert, Emrullah Korkmaz, Louis D. Jr. Falo, and Steven R. Little. Microfluidic Systems For Manufacturing of Microparticle-Based Drug-Delivery Systems: Design, Construction, and Operation. *ACS Biomaterials Science & Engineering*, 8(7):2864–2877, July 2022. doi: 10.1021/acsbiomaterials.2c00066.
5. Chak Ming Leung, Pim de Haan, Kacey Ronaldson-Bouchard, Ge-Ah Kim, Jihoon Ko, Hoon Suk Rho, Zhu Chen, Pamela Habibovic, Noo Li Jeon, Shuichi Takayama, Michael L. Shuler, Gordana Vunjak-Novakovic, Olivier Frey, Elisabeth Verpoorte, and Yi-Chin Toh. A guide to the organ-on-a-chip. *Nature Reviews Methods Primers*, 2(1):1–29, May 2022. ISSN 2662-8449. doi: 10.1038/s43586-022-00118-6.
6. Leyla Amirifar, Amir Shamloo, Rohollah Nasiri, Natan Roberto de Barros, Ze Zhong Wang, Bige Deniz Unluturk, Alberto Libanori, Oleksandr Ievglevskyi, Sibel Emir Diltemiz, Samuel Sances, Ilangko Balasingham, Stephanie K. Seidlits, and Nureddin Ashammakhi. Brain-on-a-chip: Recent advances in design and techniques for microfluidic models of the brain in health and disease. *Biomaterials*, 285:121531, June 2022. ISSN 0142-9612. doi: 10.1016/j.biomaterials.2022.121531.
7. Brittany N Dugger and Dennis W Dickson. Pathology of neurodegenerative diseases. *Cold Spring Harbor perspectives in biology*, 9(7):a028035, 2017.
8. David M Wilson, Mark R Cookson, Ludo Van Den Bosch, Henrik Zetterberg, David M Holtzman, and Ilse Dewachter. Hallmarks of neurodegenerative diseases. *Cell*, 186(4):693–714, 2023.
9. Anna Slanzi, Giulia Iannoto, Barbara Rossi, Elena Zenaro, and Gabriela Constantin. In vitro models of neurodegenerative diseases. *Frontiers in cell and developmental biology*, 8:328, 2020.
10. Pooja Gangras, Valentina Gelfanova, Graham D. Williams, Samuel K. Handelman, Ryan M. Smith, and Marjoke F. Debets. Investigating SH-SY5Y Neuroblastoma Cell Surfaceome as a Model for Neuronal-Targeted Novel Therapeutic Modalities. *International Journal of Molecular Sciences*, 23(23):15062, January 2022. ISSN 1422-0067. doi: 10.3390/ijms232315062.
11. Fernanda Martins Lopes, Rafael Schröder, Mário Luiz Conte da Frota Júnior, Alfeu Zanotto-Filho, Carolina Beatriz Müller, André Simões Pires, Rosalva Thereza Meurer, Gabriela Delevati Colpo, Daniel Pens Gelain, Flávio Kapczinski, et al. Comparison between proliferative and neuron-like sh-sy5y cells as an in vitro model for parkinson disease studies. *Brain research*, 1337:85–94, 2010.
12. Helena Xicoy, Bé Wieringa, and Gerard JM Martens. The sh-sy5y cell line in parkinson's disease research: a systematic review. *Molecular neurodegeneration*, 12:1–11, 2017.
13. R Constantinescu, AT Constantinescu, H Reichmann, and B Janetzky. *Neuronal differentiation and long-term culture of the human neuroblastoma line SH-SY5Y*. Springer, 2007.
14. Haya Alrashidi, Simon Eaton, and Simon Heales. Biochemical characterization of proliferative and differentiated sh-sy5y cell line as a model for parkinson's disease. *Neurochemistry International*, 145:105009, 2021.
15. Lotta Agholme, Tobias Lindström, Katarina Kågedal, Jan Marcusson, and Martin Hallbeck. An in vitro model for neuroscience: differentiation of sh-sy5y cells into cells with morphological and biochemical characteristics of mature neurons. *Journal of Alzheimer's disease*, 20 (4):1069–1082, 2010.
16. Liana M de Medeiros, Marco A De Bastiani, Eduardo P Rico, Patrícia Schonhofen, Bianca Pfaffenseller, Bianca Wollenhaupt-Aguiar, Lucas Grun, Florência Barbé-Tuana, Eduardo R Zimmer, Mauro AA Castro, et al. Cholinergic differentiation of human neuroblastoma sh-sy5y cell line and its potential use as an in vitro model for alzheimer's disease studies. *Molecular Neurobiology*, 56:7355–7367, 2019.
17. Mathias Jucker and Lary C Walker. Self-propagation of pathogenic protein aggregates in neurodegenerative diseases. *Nature*, 501(7465):45–51, 2013.
18. Jaime Vaquer-Alicea and Marc I Diamond. Propagation of protein aggregation in neurodegenerative diseases. *Annual review of biochemistry*, 88:785–810, 2019.
19. Patcharapong Pantiya, Chanisa Thonusin, Nipon Chattipakorn, and Siriporn C Chattipakorn. Mitochondrial abnormalities in neurodegenerative models and possible interventions: Focus on alzheimer's disease, parkinson's disease, huntington's disease. *Mitochondrion*, 55:14–47, 2020.
20. Hubert Grel, Damian Woznica, Katarzyna Ratajczak, Ewelina Kalwarczyk, Julia Anchimowicz, Weronika Switlik, Piotr Olejnik, Piotr Zielonka, Magdalena Stobiecka, and Slawomir Jakiela. Mitochondrial dynamics in neurodegenerative diseases: Unraveling the role of fusion and fission processes. *International Journal of Molecular Sciences*, 24(17):13033, 2023.
21. E. Kalwarczyk and S. Jakiela. Exploring cellular dynamics: A comprehensive analysis of sh-sy5y cell growth in variable polycarbonate chambers and comparative insights with standard petri dishes. *Zenodo*, page https://zenodo.org/records/10401181, 2023. doi: 10.5281/zenodo.10401181.
22. D. Woznica and S. Jakiela. Sh-sy5y cell proliferation within a hermetically sealed polycarbonate chamber for a duration of two weeks. *Zenodo*, page https://zenodo.org/records/10418022, 2023. doi: 10.5281/zenodo.10418022.
23. Amar Singh, Arghya Maity, and Navin Singh. Structure and Dynamics of dsDNA in Cell-like Environments. *Entropy*, 24(11):1587, November 2022. ISSN 1099-4300. doi: 10.3390/e24111587.
24. Martin D Brand and David G Nicholls. Assessing mitochondrial dysfunction in cells. *Biochemical Journal*, 435(2):297–312, 2011.
25. M. Stiehler, C. Bünger, A. Baatrup, M. Lind, M. Kassem, and T. Mygind. Effect of dynamic 3-d culture on proliferation, distribution, and osteogenic differentiation of human mesenchymal stem cells. *Journal of Biomedical Materials Research Part A*, 89A:96–107, 2008. doi: 10.1002/jbm.a.31967.
26. I. Vlodavsky, R. Voss, S. Yarkoni, and Z. Fuks. Stimulation of human amniotic fluid cell proliferation and colony formation by cell plating on a naturally produced extracellular matrix. *Prenatal Diagnosis*, 2:13–23, 1982. doi: 10.1002/pd.1970020104.
27. Kaitlyn E. Johnson, Grant Howard, William Mo, Michael K. Strasser, Ernesto A. B. F. Lima, Sui Huang, and Amy Brock. Cancer cell population growth kinetics at low densities deviate from the exponential growth model and suggest an Allee effect. *PLOS Biology*, 17(8): e3000399, August 2019. ISSN 1545-7885. doi: 10.1371/journal.pbio.3000399. Publisher: Public Library of Science.
28. V. S. Nirmalanandhan, M. S. Levy, A. J. Huth, and D. L. Butler. Effects of cell seeding density and collagen concentration on contraction kinetics of mesenchymal stem cell–seeded collagen constructs. *Tissue Engineering*, 12:1865–1872, 2006. doi: 10.1089/ten.2006.12.1865.
29. Yan Li, Hua Xiong, and Da-Qing Yang. Functional switching of ATM: sensor of DNA damage in proliferating cells and mediator of Akt survival signal in post-mitotic human neuron-like cells. *Chinese Journal of Cancer*, 31(8):364–372, August 2012. ISSN 1000467X, 1944446X. doi: 10.5732/cjc.012.10086.
30. Susan Dwane, Edel Durack, and Patrick A. Kiely. Optimising parameters for the differentiation of SH-SY5Y cells to study cell adhesion and cell migration. *BMC Research Notes*, 6 (1):366, September 2013. ISSN 1756-0500. doi: 10.1186/1756-0500-6-366.
31. Fabian Dieter, Carsten Esselun, and Gunter P. Eckert. Redox Active $\alpha$-Lipoic Acid Differentially Improves Mitochondrial Dysfunction in a Cellular Model of Alzheimer and Its Control Cells. *International Journal of Molecular Sciences*, 23(16):9186, January 2022. ISSN 1422-0067. doi: 10.3390/ijms23169186.
32. Yong-Jun Li, Yueli Zhan, Chengrui Li, Jianhong Sun, and Chengliang Yang. CPI-1189 protects neuronal cells from oxygen glucose deprivation/re-oxygenation-induced oxidative injury and cell death. *Aging*, 13(5):6712–6723, February 2021. ISSN 1945-4589. doi: 10.18632/aging.202528.
33. Carlie Rein, Mehmet Toner, and Derin Sevenler. Rapid prototyping for high-pressure microfluidics. *Scientific Reports*, 13(1):1232, January 2023. ISSN 2045-2322. doi: 10.1038/s41598-023-28495-2.


DRAFT